JOURNAL OF Applied Polymer SCIENCE

Impact of nanoclay on physicomechanical and thermal analysis of polyvinyl alcohol/fumed silica/clay nanocomposites

Josephine Chang-Hui Lai,[1] Md. Rezaur Rahman,[1] Sinin Hamdan,[2] Fui Kiew Liew,[2] Md. Mizanur Rahman,[1] Md. Faruk Hossen[1]

[1]Department of Chemical Engineering and Energy Sustainability, Faculty of Engineering, Universiti Malaysia Sarawak, Kota Samarahan, Sarawak 94300, Malaysia

[2]Department of Mechanical Engineering, Faculty of Engineering, Universiti Malaysia Sarawak, Kota Samarahan, Sarawak 94300, Malaysia

Correspondence to: J. C.-H. Lai (E-mail: josephinelai91@hotmail.com)

ABSTRACT: Polyvinyl alcohol (PVA)/fumed silica/clay nanocomposites are prepared via solution intercalation by exploiting phase separation based on the bridging of particles by polymer chains. PVA/fumed silica/clay nanocomposites are characterized by Fourier transform infrared spectroscopy (FTIR), scanning electron microscopy, and thermogravimetric analysis. Mechanical properties are determined by universal testing machine. From FTIR results, it indicates that IR spectrum for PVA/fumed silica/clay nanocomposites, especially PVA/fumed silica/clay (1.30E) nanocomposites, is much broader than pure PVA and other clay nanocomposites. The better interfacial bonding between PVA/fumed silica/clay (1.30E) nanocomposites are reflected in the improvement of the mechanical properties as well as thermal stability. The surface area analysis result proves that the PVA/fumed silica/clay (1.30E) nanocomposites have higher surface area and pore volume with less pore size. With the addition of 1.30E clay to the composite system, the tensile strength and modulus had shown the highest values as well as higher activation energy for thermal decomposition. © 2014 Wiley Periodicals, Inc. J. Appl. Polym. Sci. **2015**, *132*, 41843.

KEYWORDS: clay; thermogravimetric analysis; mechanical properties

Received 3 September 2014; accepted 2 December 2014
DOI: 10.1002/app.41843

INTRODUCTION

Nowadays, polyvinyl alcohol (PVA) is commonly used as a binder in the preparation of ceramics and can be used as a copolymer of pyroelectric films or for medical purposes.[1,2] PVA can be used in membrane separation, drug delivery systems, artificial biomedical devices, and fuel cell electrolytes.[3–8] However, PVA is not applicable to the aqueous environment as it has hydrophilic nature.[9] The incorporation of filler materials into PVA matrix will enhance the mechanical strength of the polymer composite.[10–12]

Besides, silicon dioxide has been largely used as filler to improve the properties of polymers. Fumed silica can be defined as finely divided amorphous silicon dioxide particles produced by high temperature in an oxygen–hydrogen flame.[13,14] Because a large number of silanols are not hydrogen-bonded, they are isolated and distributed over the surface, and this leads to approximately every second silicon atom on the fumed silica surface to bear a silanol group.[13,15,16]

In addition to that clay plays an important role in the production of polymer composites. Clays are defined as a group of materials with high impact on polymer composite research.[17] The most commonly used clay, namely, montmorillonite (MMT), has shown to improve the physical and mechanical properties of nanocomposites.[18]

Polymer nanocomposites present a very attractive route to upgrade and diversify properties of the polymers. In the modern research, polymer nanocomposites exhibit significant improvement on mechanical properties and thermal properties, which apply for biomedical application like drug delivery system. Polymer–clay nanocomposites (PCNs) are considered as a new class of organic–inorganic hybrid materials. There are many advantages of using PCNs, such as improved modulus and strength, high heat distortion temperature, high specific stiffness, good thermal stability, and reduced gas permeability at low filler concentrations.[19–21]

Furthermore, the highly dispersed fumed silica enhances the thermal properties in polymer/clay composite systems.[14,15] The fumed silica nanopowder acts as filler in polymer composites, which enhances tensile strength, impact strength, and thermal stability.[22] Nanoclay itself has an important role in the polymer/

clay nanocomposites system, that is, the tensile modulus, tensile strength, and elongation at break of the composites increased with the loading of nanoclay up to 3%; however, the impact strength decreased with higher loading of nanoclay.[23] The modification of clay by ammonium ion with trihydroxyl groups provides more tethering points with polyurethane molecules than clay treated by ammonium ion with monohydroxyl and dihydroxyl groups, which enhances the mechanical properties of polymer composites.[24]

Therefore, this study investigated the effect of fumed silica and different types of clays on thermal and mechanical properties of PVA/fumed silica/clay nanocomposites. The physical, mechanical, and thermal properties of pure PVA and PVA/fumed silica/clay nanocomposites were characterized. The compatibility of different types of clays with PVA/fumed silica is also reported.

MATERIALS AND METHODS

Materials

The silicon dioxide powders used were supplied by Sigma-Aldrich. Catalog number of the powders was S5631-500G. The particle size of silicon dioxide powder is less than 8 μm, and it is white to off-white in color. The chemicals PVA, Nanoclay, Nanomer 1.28E, 1.30E, 1.31PS, and 1.34TCN used were supplied by Sigma-Aldrich. Nanomer 1.28E was MMT clay surface modified with 25–30 wt % trimethyl stearyl ammonium. The bulk density of the clay was 200–500 kg/m^3, and the average particle size was around 20 μm. Nanomer 1.30E was MMT clay surface modified with 25–30 wt % octadecylamine. The bulk density of the clay was 200–500 kg/m^3, and the average particle size was around 20 μm. Nanomer 1.31PS was MMT clay surface modified with 15–35 wt % octadecylamine and 0.5–5 wt % aminopropyltriethoxysilane. The bulk density of the clay was 200–500 kg/m^3, and the average particle size was around 20 μm. Nanomer 1.34TCN was MMT clay surface modified with 25–30 wt % methyl dihydroxyethyl hydrogenated tallow ammonium. The bulk density of the clay was 200–500 kg/m^3, and the average particle size was around 20 μm.

Monomer Preparation

The monomer system was prepared using PVA without any initiator. About 27.0 g of PVA, 0.5 g of nanoclay, and 2.5 g of fumed silica were prepared as shown in Table I.

Solution Intercalation of the PVA/Fumed Silica/Clay Nanocomposites

PVA and clay were dried at 50 and 60°C, respectively, for 24 h in a vacuum oven. The samples were prepared in a deionized water/methanol (3 : 1) solvent mixture. The mixtures mixed together with fumed silica were first stirred at 70°C for 24 h. Then, the homogeneous solutions were ultrasonicated in an ultrasonic bath at room temperature for 1 h. Solid films were produced by casting a sample onto a glass mold by slowly evaporating the solvent in air for 3 days. The films with a thickness of ~ 150 μm were put in a vacuum oven at 50°C for 24 h to get rid of the extra solvent. The dried films were stored in desiccators prior to any characterization.

Microstructural Analysis

Fourier Transform Infrared Spectroscopy. The infrared spectra of the monomer systems were recorded on a Shimadzu IR Affinity-1. The transmittance range of the scan was 700–4000 cm^{-1}.

Table I. Preparation of Monomer System with Different Types of Nanoclay

Amount of polyvinyl alcohol (g)	Amount of fumed silica (g)	Types of nanoclay (g)
30	0	0
27	2.5	0.5 (1.28E)
27	2.5	0.5 (1.30E)
27	2.5	0.5 (1.31PS)
27	2.5	0.5 (1.34TCN)

Scanning Electron Microscopy. The interfacial bonding between PVA, clay, and silicate were examined using a scanning electron microscope (SEM; JSM-6710F) supplied by JEOL, Japan. The specimens were first fixed with Karnovsky's fixative and then taken through a graded alcohol dehydration series. Once dehydrated, the specimen was coated with a thin layer of gold before being viewed microscopically. The micrographs were taken at a magnification of range between 250× and 1500×.

Adsorption Isotherm. The nitrogen adsorption isotherm of PVA and PVA/silica/clay nanocomposites at 77 K was obtained by using a Quantachrome, Asic-7 physicosorption analyzer. In the analysis, the nanocomposites were degassed at 250°C in vacuum for 1 h before the nitrogen adsorption isotherm was constructed. The surface area and the pore volume of nanocomposites were evaluated by the Brunauer–Emmett–Teller (BET) model.

Tensile Testing. Mold-shape thin films were cut with a rectangular die and tested in a Lloyd LRX (2500 N) materials testing machine at room temperature. The gauge length was 25 mm. The width and thickness of the samples were 4 and 0.150 mm, respectively. The cross head speed was 1 mm/min. The quoted results were averaged over at least four specimens.

Thermogravimetric Analysis. Thermogravimetric analysis (TGA) measurements were carried out on 5–10 mg of both pure PVA and PVA/silica/clay nanocomposites at a heating rate of 10°C/min in a nitrogen atmosphere using a Thermogravimetric Analyzer (TA Instrument SDT Q600). Pure PVA and PVA/silica/clay nanocomposites were subjected to TGA in high-purity nitrogen under a constant flow rate of 5 mL/min. Thermal decomposition of each sample occurred in a programmed temperature range of 0–700°C. The continuous weight loss and temperature were recorded and analyzed.

RESULTS AND DISCUSSION

Fourier Transform Infrared Spectroscopy

The IR spectra of PVA and PVA/fumed silica/clay nanocomposites are shown in Figure 1. The functional groups of ν(Si—O—Si), ν(Si—OH), and δ(Si—O—Si) had their characteristic peaks between 1100–1000, 950–900, and 800–700 cm^{-1}, respectively.[25] The characteristic bands at 1650 and 1420 cm^{-1} were attributed to ν(C=C) and δ(CH_2), respectively. For the ν(CH_2) group, the IR spectrum was between 2900 and

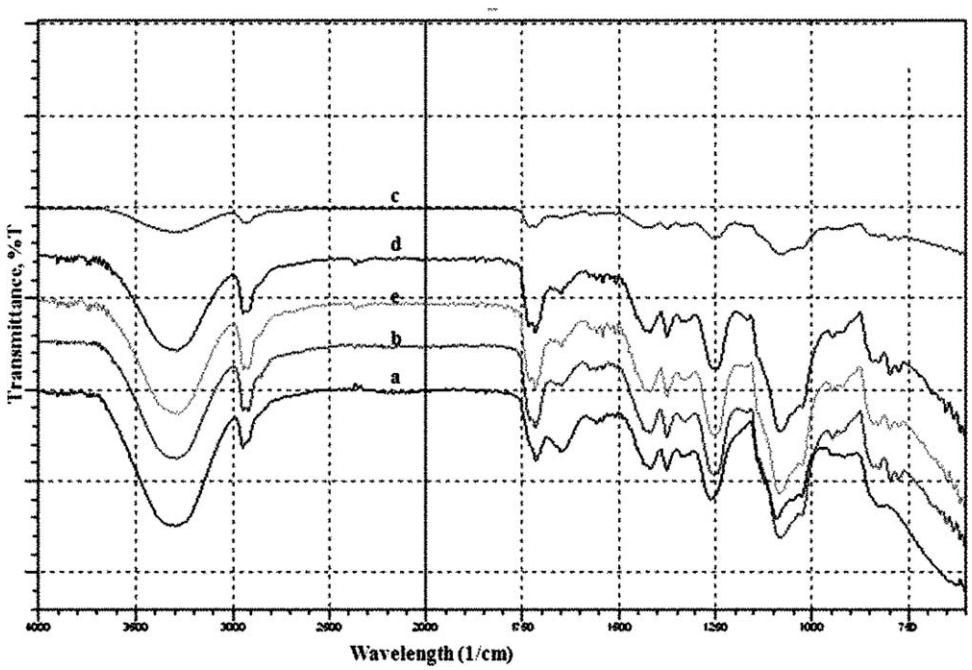

Figure 1. FTIR graphs for (a) PVA samples, (b) PVA/fumed silica/clay (1.28E) nanocomposites, (c) PVA/fumed silica/clay (1.30E) nanocomposites, (d) PVA/fumed silica/clay (1.31PS) nanocomposites, and (e) PVA/fumed silica/clay (1.34TCN) nanocomposites.

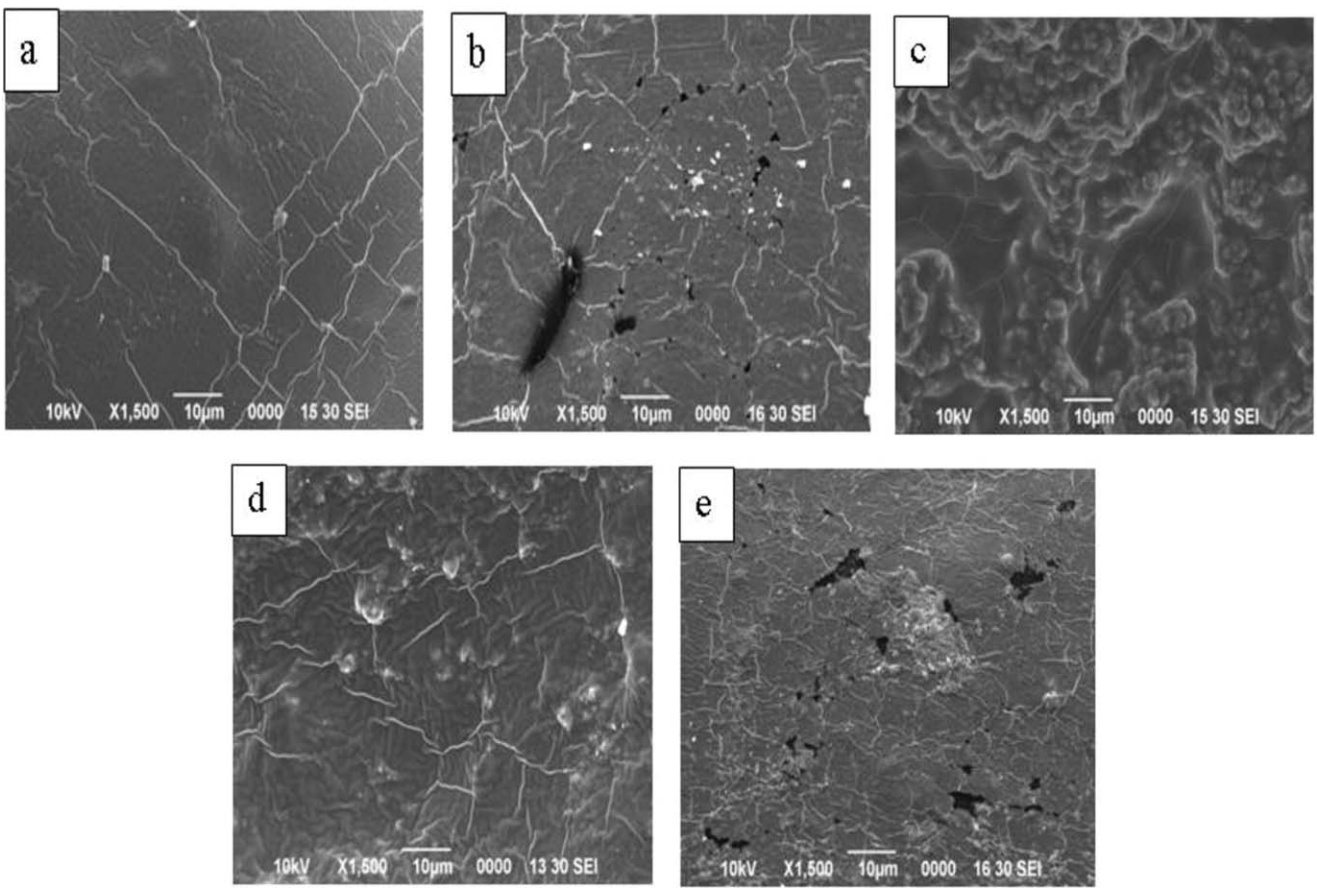

Figure 2. SEM micrographs of (a) PVA samples, (b) PVA/fumed silica/nanoclay (1.28E) nanocomposites, (c) PVA/fumed silica/nanoclay (1.30E) nanocomposites, (d) PVA/fumed silica/nanoclay (1.31PS) nanocomposites, and (e) PVA/fumed silica/nanoclay (1.34TCN) nanocomposites.

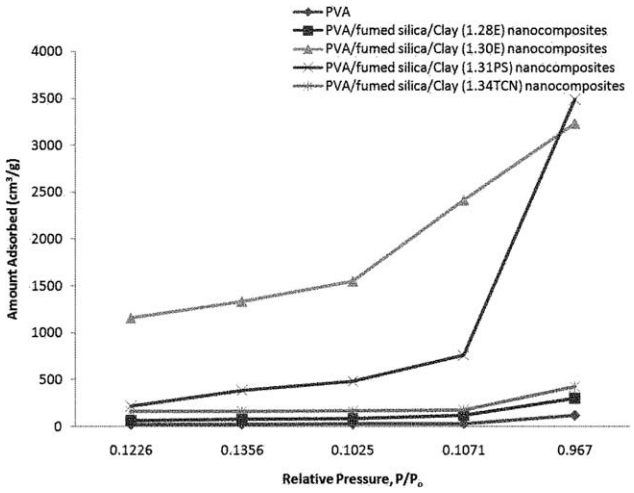

Figure 3. N_2 adsorption isotherms of PVA and PVA/fumed silica/clay nanocomposites.

3100 cm^{-1}.[26,27] According to this finding, partial loss of silanol groups bonded with silica particles, which was detected and immobilized the surface of functionalized silica nanoparticles.[28] The spectrum 950–900 cm^{-1} represented the silanol group bonds of silica nanoparticles. Because of the combination of clay and PVA coupled with silica nanoparticles, the amplitudes of Si—O—Si were increased when compared with original silica nanoparticles.

The major vibration bands at 950–900 cm^{-1} and 800–700 cm^{-1} represented the PVA/fumed silica/clay nanocomposites. The characteristic bands of 3296.35 and 2918.30 cm^{-1} proved the $\nu(OH)$ and $\nu(CH_2)$ in PVA as shown in Figure 1 (Peak a). IR spectrum for PVA/fumed silica/clay (1.30E) nanocomposites was much broader when compared with the pure PVA and other PVA/fumed silica/clay nanocomposites because of the silica nanoparticles appended at side chain hampering the formation of hydrogen bond between PVA chains. The hydroxyl group is replaced by silica group and ammonium group, as shown in Figure 1, which proved that PVA and clay are compatible with fumed silica and had altered tridimensional structure of PVA chains.[28]

Scanning Electron Microscopy

The SEM micrographs of pure PVA and aggregation of silica and clay nanocomposites are shown in Figure 2(a–e). The smooth surface morphology, as shown in Figure 2(a), indicated that there was no interfacial bonding and no monomer intercalation.[28,29] Figure 2(b–e) shows some agglomeration between PVA, fumed silica, and clay, which proved the aggregation of fumed silica in the interspherulitic region. The uniform surface of PVA/fumed silica/clay (1.30E) and PVA/fumed silica/clay (1.31PS) nanocomposites proved the compatibility among the PVA/fumed silica with clay, as shown in Figure 2(c,d). From Figure 2(b,e), it can be observed that PVA/fumed silica/clay was dispersed unevenly in the presence of agglomeration because of the high surface energy and poor adhesion between clay and PVA/fumed silica matrix. The poor compatibility of PVA/fumed silica matrix with clay occurred as the inert surface of PVA/fumed silica could not react well with the clay particles.[30] The outcome of the better interfacial bonding and strong compatibility among the PVA/fumed silica/clay (1.30E) nanocomposites was reflected in the improvement of the mechanical properties as well as thermal stability.

Adsorption Isotherm

The N_2 adsorption isotherms measured for PVA and PVA/fumed silica/clay nanocomposites are shown in Figure 3. For specific surface area, S_{BET} was calculated by the BET equation.[31] The surface areas for the pure PVA and PVA/fumed silica/clay (1.28E), (1.30E), (1.31PS), and (1.34TCN) nanocomposites were found to be 1.93, 3.81, 468.4, 167.96, and 23.54 m^2/g, respectively, which indicated an increase of surface area of nanocomposites when compared with the pure PVA. Because of the good dispersion of the nanoclay within the PVA/fumed silica matrix, the pores were decreased and enhanced their accessibility for nitrogen adsorption. The isotherm patterns showed the presence of a hysteresis loop, which was a characteristic feature of the Type IV isotherms according to the original IUPAC classification.[32,33] In the case of PVA sample, the isotherm initially showed an initial ascending section up to $P/P_o = 0.107$; afterward, it showed a rather straight section, which extended up to $P/P_o = 0.97$. Finally, the isotherm exhibited an upward sweep near saturation pressure. Similar pattern of isotherm was observed in the nanocomposites of PVA/fumed silica/clay (1.28E), (1.30E), (1.31PS), and (1.34TCN), with the initial ascending section extended up to $P/P_o = 0.107$, 0.103, 0.107, and 0.107, respectively. The enhancement in the N_2 adsorption at high P/P_o values was observed for PVA/fumed silica/clay (1.30E) nanocomposites. According to the average pore diameter (4V/A by BET), the incorporation of nanoclay into PVA/fumed silica systems, BET surface area and pore volume of PVA/fumed silica/clay (1.30E) and (1.31PS) greatly increased,

Table 2. Physical Properties Detected from N_2 Adsorption at 77 K on PVA and PVA/Fumed Silica/Clay Nanocomposites

Sample	Specific surface area, S_{BET} (m^2/g)	Average pore volume, V_m (10^{-4} cm^3/g)	d_{BET} (nm)	Type of isotherms
PVA	1.93	0.00008	2.00	IV
PVA/fumed silica/clay (1.28E) nanocomposites	3.81	0.00010	1.58	IV
PVA/fumed silica/clay (1.30E) nanocomposites	468.4	19.90000	1.57	IV
PVA/fumed silica/clay (1.31PS) nanocomposites	167.96	8.36000	1.57	IV
PVA/fumed silica/clay (1.34TCN) nanocomposites	23.54	1.99000	1.57	IV

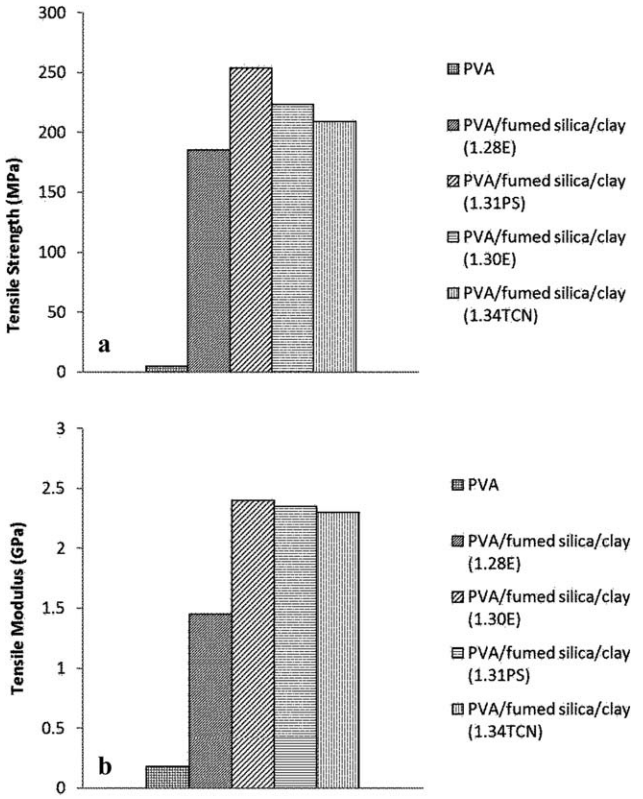

Figure 4. Tensile strength (a) and tensile modulus (b) of PVA and PVA/fumed silica/clay nanocomposites.

whereas the pore size decreased, as shown in Table 2.[34] Although the pore volume increased slightly, on the other hand, the BET surface area increased significantly, which was reflected in the decrease of pore size. The adsorption isotherms indicated that the pores were mesoporous. It proved that PVA/fumed silica/clay (1.30E) nanocomposites had the highest surface area and average pore volume with less pore size, which was reflected in the surface morphology and thermal analysis.

Tensile Testing

The tensile strength and tensile modulus of pure PVA and different types of clay-loaded PVA/fumed silica/clay nanocomposites are shown in Figure 4(a,b), respectively. As shown in Figure 4(a), all the PVA/fumed silica/clay systems had higher tensile strength when compared with the pure PVA system. Among all the composite systems, PVA/fumed silica/clay (1.30E) nanocomposites showed the highest tensile strength when compared with PVA/fumed silica/clay (1.28E) nanocomposites, PVA/fumed silica/clay (1.30E) nanocomposites, and PVA/fumed silica/clay (1.34TCN) nanocomposites. It showed that the tensile strength increased significantly when the clay was added to the PVA/fumed silica composites.[35] On the other hand, silica was left unbounded to PVA particles as the nanocomposites aggregate reduced interparticle distance.[36]

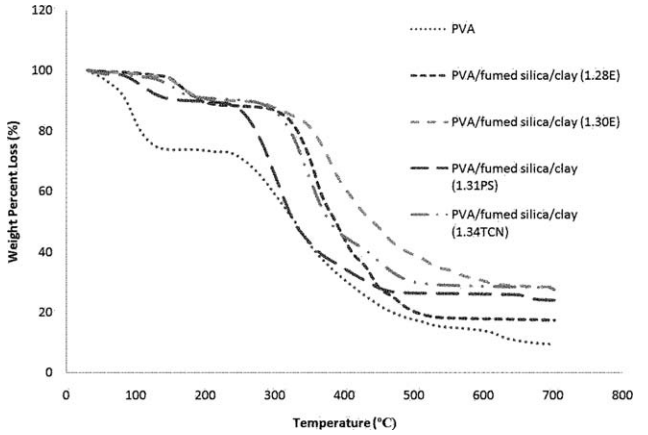

Figure 5. TGA curves for PVA sample and PVA/fumed silica/clay nanocomposites.

Figure 4(b) shows that most of the PVA/fumed silica/clay system had high tensile modulus except for PVA/fumed silica/clay (1.28E) nanocomposites. It was due to the clay (1.30E) containing octadecylamine improving the miscibility of clay and PVA system. The improved interfacial bonding can realize the load transfer from matrix to clay, which was attributed to the alkyl chains on the surface of fumed silica/clay.[35] This proved that the clay (1.30E) added to the PVA/fumed silica system increased compatibility, which enhanced the tensile strength and modulus. The outcome of the better compatibility of PVA/fumed silica/clay (1.30E) nanocomposites was reflected in the thermal stability as well as the surface morphology.

Table 3. Activation Energy of PVA Sample and PVA/Fumed Silica/Clay Nanocomposites Determined by Using Arrhenius Equation

Samples	T_i (°C)[a]	T_m (°C)[b]	T_f (°C)[c]	W_{T_i} (%)[d]	W_{T_m} (%)[e]	W_{T_f} (%)[f]	Activation Energy, E_a (kJ/mol)
PVA	236.0	326.0	347.0	72.8	50.72	43.8	20.403
PVA/fumed silica/nanoclay (1.28E) nanocomposites	280.0	347.0	410.0	89.1	66.0	43.5	25.574
PVA/fumed silica/nanoclay (1.30E) nanocomposites	303.0	431.0	511.0	86.0	52.0	38.0	31.660
PVA/fumed silica/nanoclay (1.31PS) nanocomposites	280.0	368.0	441.0	87.8	54.1	38.6	30.138
PVA/fumed silica/nanoclay (1.34TCN) nanocomposites	258.0	303.0	368.0	85.3	61.8	39.0	28.633

[a] Temperature corresponding to the beginning of decomposition.
[b] Temperature corresponding to the maximum rate of mass loss.
[c] Temperature corresponding to the end of decomposition.
[d] Mass loss at temperature corresponding to the beginning of decomposition.
[e] Mass loss at temperature corresponding to the maximum rate of mass loss.
[f] Mass loss at temperature corresponding to the end of decomposition.

Thermogravimetric Analysis

The TGA curves of PVA/fumed silica/clay nanocomposites are shown in Figure 5. Figure 5 shows that the thermal stability of different clay-loaded composites increases significantly when compared with the pure PVA. Three steps in the thermal decomposition of PVA and PVA/fumed silica/clay nanocomposites could be observed. Initial temperature of every step was defined as a critical point of weight loss for the sample in the TG curve.[37] This step was associated with the moisture loss or evaporation of trapped solvent.

According to the TGA thermograph, the weight loss was about 8.67%, 0.56%, 0.48%, 1.61%, and 1.49% for pure PVA, 1.28E, 1.30E, 1.31PS, and 1.34TCN clay-loaded nanocomposites, respectively. Different weight losses were visible because of the removal of moisture. The weight loss for second-step degradation was found to be 23.4% for PVA and about 10.0% for PVA/fumed silica/clay nanocomposites.[28] Because of the restriction in polymer mobility and suppression of decomposition, different types of clay led to different weight loss. It showed that nanoclay and silica were well intercalated with polymer matrix by covalent bonds.[28] Well-distributed silicate layers of clay could prevent the passage of volatile decomposed product throughout the composite. The addition of nanoclay and silica improved the thermal stability of nanocomposites.[38] At the final degradation, which started at 250°C and ended at 430°C, the weight loss found for PVA, 1.28E, 1.30E, 1.31PS, and 1.34TCN composites were 63.6%, 60.3%, 42.1%, 64.4%, and 54.5% respectively. The final weights of composites were significantly less than pure PVA due to the degradation temperature of silica itself being 360°C. The bonding compatibility of PVA/silica and 1.30E clay was higher than 1.28E, 1.31PS, and 1.34TCN clay nanocomposites because of the significant reduction of hydroxyl group, which is reflected in the Fourier transform infrared spectroscopy (FTIR) results.

The activation energy could be helpful in reaching conclusions about the thermal stability of PVA/fumed silica/clay nanocomposites. The Arrhenius equation was used to determine the activation energy.[39] The activation energy of PVA and PVA/fumed silica/clay nanocomposites calculated by plotting the graph is summarized in Table 3. It was found that the activation energy of PVA/fumed silica/clay nanocomposites were significantly higher than that of pure PVA. The higher activation energy implied the greater thermal stability. The PVA/fumed silica/clay (1.30E) nanocomposites had higher activation energy when compared with the pure PVA and PVA/fumed silica/clay (1.34TCN) nanocomposites.

CONCLUSIONS

PVA/fumed silica/clay nanocomposites were prepared via solution intercalation. The reduction of hydroxyl group and the dispersion of clay were confirmed by FTIR spectroscopy. The surface morphology showed that the coated surface becomes more hydrophobic with increasing clay content, which meant that clay imparted antiwetting property to the hybrid films. The surface analysis result proved that the PVA/fumed silica/clay nanocomposites had higher surface area and pore volume with less pore size. It also proved that the clay added to the PVA/fumed silica (1.30E) system was compatible which enhanced the tensile strength and modulus. Nanoclay dispersion in PVA/fumed silica nanocomposite increased the thermal stability with increasing weight percentage of the clay content. The thermal stability of PVA/fumed silica/clay (1.30E) nanocomposites was the highest with higher activation energy. The outcome of the better compatibility of PVA/fumed silica/clay (1.30E) nanocomposites was reflected in the thermal stability results and surface morphology analysis.

ACKNOWLEDGMENTS

This work received financial support from the Ministry of Higher Education Malaysia [Grant no. ERGS/02 (08)/860/2912(12)].

REFERENCES

1. Szafran, M.; Wisniewski, P.; Rokicki, G. *J. Therm. Anal. Calorim.* **2004**, *77*, 319.
2. Frubing, P.; Wegener, M.; Gerhard-Multhaupt, R.; Buchsteiner, A.; Neumann, W.; Brehmer, L. *Polymer* **1999**, *40*, 3413.
3. Kusumocahyo, S. P.; Sano, K.; Sudoh, M.; Kensaka, M. *Sep. Purif. Technol.* **2000**, *18*, 141.
4. Gref, G.; Nyugen, Q. T.; Schaetzel, P.; Neel, J. *J. Appl. Polym. Sci.* **1993**, *49*, 209.
5. Narashimhan, B. Mathematical models describing polymer dissolution: consequences for drug delivery. *Adv. Drug Deliv. Rev.* **2001**, *48*, 195.
6. Razzak, M. T.; Zainuddin, E.; Dewi, S. P.; Lely, H.; Taty, E. S. *Radiat. Phys. Chem.* **1999**, *55*, 153.
7. Palacios, I.; Castillo, R.; Vargas, R. A. *Electrochim. Acta* **2003**, *48*, 2195.
8. Yang, C. C. *Mater. Sci. Eng. B* **2006**, *131*, 256.
9. Uragami, T.; Okazaki, K.; Matsugi, H.; Miyata, T. *Macromolecules* **2002**, *35*, 9156.
10. Sairan, M.; Patil, M. B.; Veerapur, R. S.; Patil, S. A.; Aminabhavi, T. M. *J. Membr. Sci.* **2006**, *281*, 95.
11. Adoor, S. G.; Sairam, M.; Manjeshwar, L. S.; Raju, K. V. S. N.; Aminabhavi, T. M. *J. Membr. Sci.* **2006**, *285*, 182.
12. Park, I.; Peng, H.-G.; Gidley, D. W.; Xue, S.; Pinnavaia, T. *J. Chem. Mater.* **2006**, *18*, 650.
13. Barthel, H. *Colloid Surf. Physicochem. Eng. Aspect* **1995**, *101*, 217.
14. Gun'ko, V. M.; Zarko, V. I.; Leboda, R.; Chibowski, E. *Adv. Colloid Interface Sci.* **2001**, *91*, 1.
15. Torro-Palau, A. M.; Fernandez-Garcia, J. C.; Orgiles-Barcelo, A. C.; Martin-Martinez, J. M. *Int. J. Adhes. Adhesive* **2001**, *21*, 1.
16. Jauregui-Beloqui, B.; Fernandez-Garcia, J. C.; Orgiles-Barcelo, A. C.; Mahiques-Bujanda, M. M.; Martin-Martinez, J. M. *Int. J. Adhes. Adhesive* **1999**, *19*, 321.
17. Garcia-Chavez, K. I.; Hernandez-Escobar, C. A.; Flores-Gallardo, S. G.; Soriano-Corral, S.; Saucedo-Salazar, E.; Zaragoza-Contreras, E. A. *Microns* **2003**, *49*, 21.

18. Yang, R. T.; Tharappiwattananon, N.; Long, R. Q. *J. Appl. Catal. B. Environ.* **1998**, *19*, 289.
19. Lu, C.; Mai, Y.-W. *Phys. Rev. Lett.* **2005**, *95*, 088303.
20. Hao, L.; Yunzhao, Y.; Yukun, Y. *Eur. Polym. J.* **2005**, *41*, 2016.
21. Xu, Y.; Brittain, W. J.; Vaia, R. A.; Price, G. *Polymer* **2006**, *47*, 4564.
22. Zheng, Y.; Zheng, Y.; Ning, R. *Mater. Lett.* **2003**, *57*, 2940.
23. Kord, B. *J. Thermoplast. Compos. Mater.* **2012**, *25*, 793.
24. Tien, Y. I.; Wei, K. H. *Macromolecules* **2001**, *34*, 9045.
25. Mansur Herman, S.; Orefice Rodrigo, L.; Mansur Alexandra, A. P. *Polymer* **2004**, *45*, 7193.
26. Perrira, A. P. V.; Vasconcelis, W. L.; Orefice Rodrigo, L. *J. Non-Cryst. Solids* **2000**, *273*, 180.
27. Liu, P.; Tian, J.; Liu, W. M. *Chin. J. Chem. Phys.* **2003**, *16*, 481.
28. Jia, X.; Li, Y.; Cheng, Q.; Zhang, S.; Zhang, B. *Eur. Polym. J.* **2007**, *43*, 1123.
29. Bhattacharya, M.; Chaudhry, S. *Mater. Sci. Eng. C* **2013**, *33*, 2601.
30. Luo, Y.; Zhao, Y.; Cai, Y.; Du, S. *Mater. Des.* **2012**, *33*, 405.
31. Brunauer, B.; Emmett, P. H.; Teller, E. *J. Am. Chem. Soc.* **1938**, *60*, 309.
32. Sing, K. S. W.; Everett, D. H.; Haul, R. A. W.; Moscou, L.; Pierotti, R. A.; Rouquerol, J.; Siemieniewska, T. *Pure Appl. Chem.* **1985**, *57*, 603.
33. Gregg, S. J.; Sing, K. S. W. Adsorption, Surface Area and Porosity, 2nd ed.; Academic Press: London, **1982**.
34. Hasan, M.; Banerjee, A. N.; Lee, M. *J. Ind. Eng. Chem.* **2014**, http://dx.doi.org/10.1016/j.jiec.2014.04.019
35. Yang, J.; Hu, J.; Wang, C.; Qin, Y.; Guo, Z. *Macromol. Mater. Eng.* **2004**, *289*, 828.
36. Nakane, K.; Yamashita, T.; Iwakura, K.; Suzuki, F. *J. Appl. Polym. Sci.* **1999**, *74*, 133.
37. Liu, Z.; Jiang, Z.; Fei, B.; Liu, X. *Bioresources* **2013**, *8*, 5014.
38. Nourbakhsh, A.; Karegarfard, A.; Ashori, A.; Nourbakhsh, A. *J. Thermoplast. Compos. Mater.* **2010**, *23*, 169.
39. Chanmal, C. V.; Jog, J. P. *eXPRESS Polym. Lett.* **2008**, *2*, 294.